High Power Laser Science and Engineering, (2018), Vol. 6, e63, 6 pages.

doi:10.1017/hpl.2018.65

All-optical μ^- acceleration in the laser wakefield

F. Zhang[1], Z. G. Deng[1], L. Q. Shan[1], Z. M. Zhang[1], B. Bi[1], D. X. Liu[1], W. W. Wang[1], Z. Q. Yuan[1], C. Tian[1], S. Q. Yang[1], B. Zhang[1], and Y. Q. Gu[1,2]

[1]*Science and Technology on Plasma Physics Laboratory, Laser Fusion Research Center, China Academy of Engineering Physics, Mianyang 621900, China*

[2]*IFSA Collaborative Innovation Center, Shanghai Jiao Tong University, Shanghai 200240, China*

(Received 5 July 2018; revised 29 September 2018; accepted 13 November 2018)

Abstract

Muons produced by the Bethe–Heitler process from laser wakefield accelerated electrons interacting with high Z materials have velocities close to the laser wakefield. It is possible to accelerate those muons with laser wakefield directly. Therefore for the first time we propose an all-optical 'Generator and Booster' scheme to accelerate the produced muons by another laser wakefield to supply a prompt, compact, low cost and controllable muon source in laser laboratories. The trapping and acceleration of muons are analyzed by one-dimensional analytic model and verified by two-dimensional particle-in-cell (PIC) simulation. It is shown that muons can be trapped in a broad energy range and accelerated to higher energy than that of electrons for longer dephasing length. We further extrapolate the dependence of the maximum acceleration energy of muons with the laser wakefield relativistic factor γ and the relevant initial energy E_0. It is shown that a maximum energy up to 15.2 GeV is promising with $\gamma = 46$ and $E_0 = 1.45$ GeV on the existing short pulse laser facilities.

Keywords: laser wakefield acceleration; muon source

1. Introduction

The muon[1] plays a key role in particle physics and applied physics, such as the muon anomalous magnetic dipole moment $a \equiv (g-2)/2$ measurement[2], muon collider and neutrino physics[3], muon catalyzed fusion[4], muon probe of the microscopic magnetic properties of materials[5], and muon radiography[6]. However, muon physics is limited by either the low flux cosmic-ray muons[7] or high cost accelerator muons[8–11].

Laser wakefield acceleration (LWFA), which promises the next generation compact high-energy electron beam source[12, 13], could also have potential application in muon source researches. While electrons can be simply self-injected through wave-breaking, an external injection is needed for muons. Such external muons could be conveniently supplied by the Bethe–Heitler lepton pair production $\gamma + A \rightarrow A' + \mu^+\mu^-$ proposed by Titov *et al.*[14], where the high-energy photons come from the LWFA electrons with energy up to several GeV[15–20] interacting with high Z materials. 10^6 dimuons could be produced by a 100 J petawatt laser facility[14] and diagnosed efficiently[21]. But those muons with lower mean energies and broad energy spread ranging from hundreds of MeV to GeV[14] limit the applications. On the other hand, those muons could be accelerated by the laser wakefield, called 'bubble', since the velocities are close or even higher than that of the bubble. Therefore for the first time we suggest an all-optical muon acceleration scheme as shown in Figure 1, in which muons could be generated by the Bethe–Heitler process via high-energy photons from the Bremsstrahlung radiation of the LWFA electrons interacting with the high Z materials, called 'Generator', and boosted by another laser wakefield, called 'Booster'.

This new all-optical 'Generator and Booster' scheme can supply a prompt, compact, low cost and controllable muon source which would have potential applications in muon collider, neutrino physics and Higgs Factory[3], muon acceleration in cosmic-ray sources[22] and other related muon physics. Peano *et al.* also proposed a scheme[23] to accelerate 'cold' muons by a slow ponderomotive beat-wave structure driven by two counterpropagating laser beams with variable frequencies which is quite different from the scheme proposed here.

In the scheme, the Generator would produce a muon bunch with short pulse duration, small source emittance and continuous energy distribution[14]. In principle, muons

Correspondence to: Y. Q. Gu, Science and Technology on Plasma Physics Laboratory, Laser Fusion Research Center, CAEP, P.O. Box 919-986, Mianyang 621900, China. Email: yqgu@caep.cn

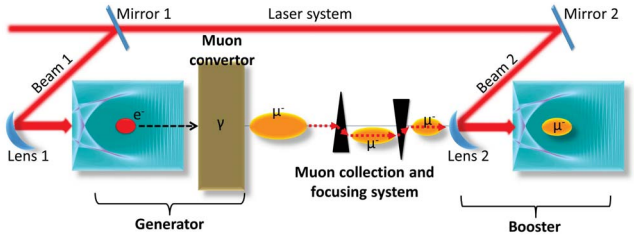

Figure 1. All-optical 'Generator and Booster' scheme of muon source. Muons are first generated by the Bethe–Heitler process, the 'Generator', via high-energy photons from Bremsstrahlung radiation of laser wakefield accelerated electrons interacting with high Z materials. After a proper collection and focusing system, muons are boosted by another laser wakefield, the 'Booster'.

produced in the Generator could be collected and focused to adapt the bubble's size before injecting into the Booster by the plasma lens[24, 25] or magnetic quadrupoles lens[26]. The time synchronization between Generator and Booster is also guaranteed in such an all-optical system. However, the huge invariant mass difference by a factor of 207 ($m_\mu = 105.7\ \mathrm{MeV}/c^2$) would result in different behaviors of muons compared to electron and positron accelerations in the bubble[27, 28]. Therefore, considering the continuous energy[14], the acceleration performance and phase matching of muons in the accelerated field of the bubble need to be studied in detail. It is worth to mention that the μ^- acceleration would be easier than that of μ^+ in a nonlinear (bubble/blow-out) regime since the accelerating/focusing wakefields for μ^- determined by background plasma density are much challenging for μ^+ same as in the cases of positrons[29]. In this paper, we focus on the μ^- acceleration. Hereafter in this paper muon denotes μ^-.

In this paper, we investigate the trapping and acceleration of muons with continuous energy distribution from the 'Generator'. The motion of muons is analyzed by one-dimensional analytic model and verified by two-dimensional particle-in-cell (PIC) simulation of a typical laser wakefield. It is shown that muons can be trapped in a broad energy range and accelerated to higher energy than that of electrons for longer dephasing length. We further extrapolate the muon acceleration to anticipate a muon energy up to 15.2 GeV on the existent short pulse laser facilities, which is exciting for the application in the laser laboratories.

2. Muon motion in one-dimensional analytic model

We first illustrate a typical laser wakefield in Figure 2(a) using the two-dimensional PIC simulation code Opic2D. A linearly polarized pulse of wavelength $\lambda_0 = 0.8\ \mu\mathrm{m}$, normalized peak amplitude $a_0 = 2$, pulse duration 33 fs and full width at half-maximum (FWHM) spot size 18 μm enters from the left of the simulation box of size $100\lambda_0 \times 60\lambda_0$. A plasma of electron density $2.2 \times 10^{18}\lambda_0^{-2}\ \mathrm{cm}^{-3}$ ($0.002n_c$) is located in $40\lambda_0 < x < 100\lambda_0$. There are 4000 × 600 cells

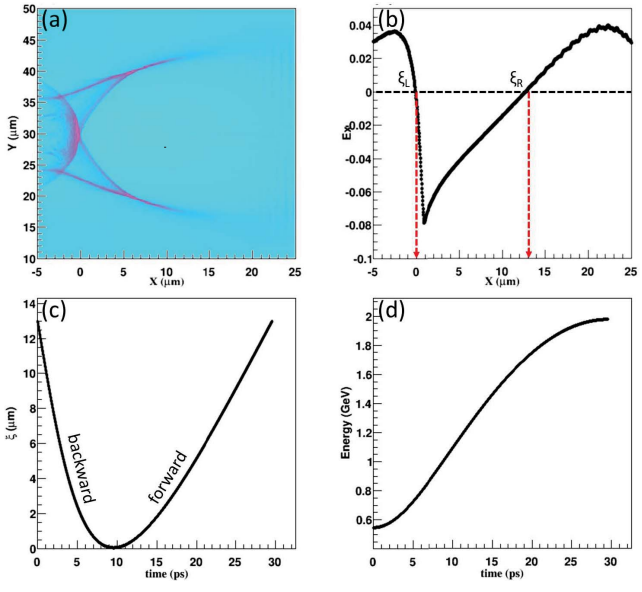

Figure 2. (a) The bubble's electron density and (b) electrostatic field in the simulation box were obtained from a two-dimensional particle-in-cell simulation code Opic2D for a plasma density $2 \times 10^{-3}n_c$. The laser pulse of wavelength 0.8 μm, normalized peak amplitude $a_0 = 2$, pulse duration 33 fs and FWHM spot size 18 μm entered from the left of the simulation box in the x direction. A muon with critical trapping energy entered into the simulation box following the trajectory shown in (c) and the energy increasing process in (d).

in the simulation windows. The particle number per cell is 4 for both electron and muon. Open boundaries are applied in both longitudinal and transverse directions. A moving window is applied in the simulation with velocity v_p which is consistent with the laser group velocity (normalized by the light speed c) reading from the simulation. The lineout on-axis electrostatic field in the moving window (i.e., in the rest frame of the bubble) is shown in Figure 2(b).

We analyze the motion of muons in such a laser wakefield in a one-dimensional analytic model. Similar as electrons, only muons locate in $\xi_L < \xi < \xi_R$ in the electrostatic field shown in Figure 2(b) are accelerated. The two zero points of $E(\xi)$ are defined as $\xi_L = 0\ \mu\mathrm{m}$ and $\xi_R = 13\ \mu\mathrm{m}$ with ξ denoting the position in the rest frame of the bubble. Considering the initial energy of muons E_0 and position ξ_0, the position of the muon in the rest frame of the bubble is

$$\xi(t) = \xi_0 + \int (v_\mu - v_p)\,\mathrm{d}t, \tag{1}$$

where the muon velocity $v_\mu = v_\mu(t)$ can be written as

$$v_\mu(t) = \left\{1 - \frac{1}{[\gamma_0 + \int E(\xi) q v_\mu(t)\,\mathrm{d}t/m_\mu]^2}\right\}^{1/2}, \tag{2}$$

where $\gamma_0 = E_0/m_\mu + 1$ is the relativistic factor with the muon mass $m_\mu = 105.7\ \mathrm{MeV}/c^2$, charge $q = -1$, and $E(\xi)$ reads from Figure 2(b). Because the muon is heavier than the electron by a factor of 207, the velocity of accelerated muons

https://doi.org/10.1017/hpl.2018.65 Published online by Cambridge University Press

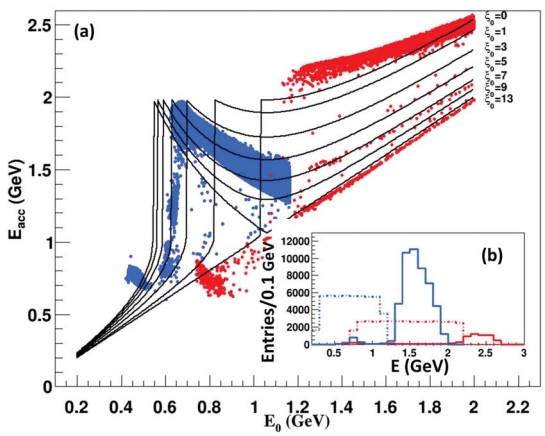

Figure 3. (a) The estimated acceleration energy of muons $E_{\rm acc}$ depending on the initial energy E_0 with different positions in the rest frame of bubble $\xi_0 \in [0, 1, 3, 5, 7, 9, 13]$ μm from the one-dimensional analytical model denoted by the solid lines. Clearly trapping energy thresholds presented from the sharp peaks of the lines. The two-dimensional PIC simulations of the forward (red dots) and backward (blue dots) muons at $t = 33$ ps show well agreement with the one-dimensional estimation. (b) The inner plot shows the spectra of the forward (red lines) and backward (blue lines) muons, where dashed lines denote the initialized energy spectra and the solid lines denote the acceleration energy spectra at $t = 33$ ps.

is lower than that of electrons which is generally taken as the light speed c.

For convenience, we define forward phase ($v_\mu > v_p$) and backward phase ($v_\mu < v_p$) denoting the initial direction of the muon in the rest frame of the bubble as shown in Figure 2(c). Giving finite laser and plasma condition, the trapping condition of muons is $v_\mu = v_p$ at $\xi = \xi_L$. Therefore, backward muons should be located at $\xi = \xi_R$ to achieve sufficient acceleration. As an example, a backward muon with critical trapping energy located at $\xi_0 = \xi_R$ would fall back to $\xi = \xi_L$ in the rest frame of the bubble with velocity climbing up to v_p. After that the muon turns into forward phase until flying over the bubble region. The whole process would follow the trajectory shown in Figure 2(c) and the energy increasing in Figure 2(d).

Then the trajectories of muons giving E_0 and ξ_0 can be calculated with this analytic model. Giving $\xi_L < \xi_0 < \xi_R$, we choose the E_0 randomly from 0.2 GeV to 2.0 GeV. When muons drop into $\xi < \xi_L$ or $\xi > \xi_R$ regions, the final acceleration energy is recorded as $E_{\rm acc}$. We calculate the trajectories for $\xi_0 \in [0, 1, 3, 5, 7, 9, 13]$ μm which are solid lines in Figure 3(a). Clearly energy thresholds for trapping $E_c(\xi_0)$ are presented by the sharp peaks of the lines. Muons located at $\xi_L = 0$ μm have the highest trapping energy threshold $E_c(\xi_L) = 1.06$ GeV and $\xi_R = 13$ μm the lowest $E_c(\xi_R) = 0.55$ GeV. Here we take $\xi_0 = \xi_R$ and $\xi_0 = \xi_L$ cases to discuss the acceleration pictures of muons in such an electrostatic field.

For $\xi_0 = \xi_R$ case, $E_0 < E_c(\xi_R)$ muons would drop out of the bubble as $v_\mu < v_p$ when falling back to $\xi = \xi_L$ and $E_0 > E_c(\xi_R)$ muons change to forward phase before falling back to $\xi = \xi_L$ resulting in insufficient acceleration, which illustrate the decline from the maximum acceleration energy. For higher $E_0 > E_c(\xi_L)$, muons dephase directly. Thus the lowest boundary of the solid line in Figure 3(a) corresponds to $E_{\rm acc} = E_0$.

For $\xi = \xi_L$ case, $E_0 < E_c(\xi_L)$ muons drop out of the bubble without trapping. It is worth to mention that muons with higher energy ($E_0 > E_c(\xi_L)$) would dephase more quickly resulting in less energy gain than the $E_0 = E_c(\xi_L)$ case. As a result, the energy spread of muons would be narrowed.

For $\xi_L < \xi < \xi_R$ case, lines stand above the $E_{\rm acc} = E_0$ boundary (the lowest boundary in Figure 3(a)) which means in a broad energy range $E_0 > E_c(\xi)$ muons could be accelerated efficiently as our expectation. The reason is even with such a broad energy spread, the velocity of muons can still follow a narrow velocity distribution adapting to the bubble's velocity.

3. Muon motion in the two-dimensional PIC simulation

With the estimation of the one-dimensional analytic model, we choose a flat energy distribution range from 0.7 GeV to 2.2 GeV with initial position $\xi \in [0, 1]$ μm denoting the forward muons and energy range from 0.2 GeV to 1.2 GeV with initial position $\xi \in [10, 13]$ μm denoting the backward muons in the two-dimensional PIC simulation. The muons are located in 18 μm $< y <$ 42 μm in the transverse direction with a density of $2\times10^{-8} n_c$ (roughly 5×10^4 muons located in a π μm $\times$ 12^2 μm $\times$ 3 μm plate), which is lower enough to avoid disturbing the bubble's plasma structure. In the simulation, we trigger the movement of muons in x direction when the bubble structure is formed. The snapshots in Figure 4 show the acceleration processes of these two groups of muons at $t = 0.33$ ps, 1.65 ps, 16.5 ps and 33 ps, respectively.

We see in Figure 4(a), at $t = 0.33$ ps, that a typical electron bubble structure is formed. The forward muons (red dots) and backward muons (blue dots) are located around the initial positions. At $t = 1.65$ ps in Figure 4(b), the backward muons are focused by the transversal field E_y. Part of the forward and backward muons with lower energy have dropped out of the bubble from the left side ($\xi < 0$). At $t = 16.5$ ps in Figure 4(c), both forward and backward muons are accelerated in the bubble sufficiently. However, the bubble structure has become unstable for the perturbation of laser transmission in the plasma. Finally at $t = 33$ ps in Figure 4(d), the bubble structure is almost absent. Both of the forward and backward muons fly freely. The x-p_x and y-p_y phase spaces of forward (red dots) and backward (blue dots) muons at the four snapshots are also shown, respectively, in Figure 4(e)–4(l). The oscillations of the two groups of muons in the y-p_y phase space present effective constraints by the transversal field E_y which would result in fine beam collimation.

https://doi.org/10.1017/hpl.2018.65 Published online by Cambridge University Press

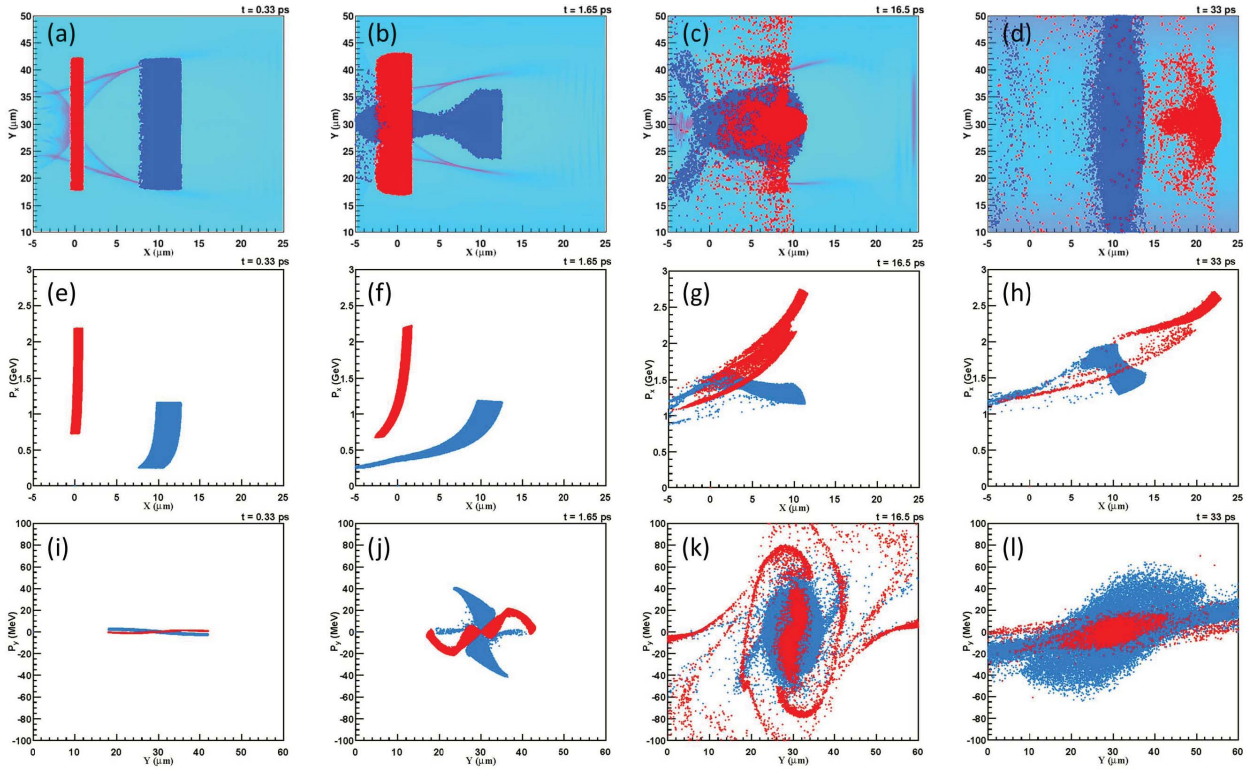

Figure 4. The snapshots of the acceleration processes of forward (red dots) and backward (blue dots) muons from the two-dimensional PIC simulations in Figure 2 at (a) $t = 0.33$ ps, (b) 1.65 ps, (c) 16.5 ps and (d) 33 ps. (e)–(h) The x-p_x and (i)–(l) y-p_y phase spaces of forward (red dots) and backward (blue dots) muons at the four snapshots are also shown, respectively.

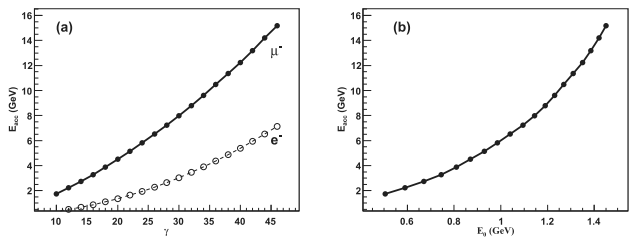

Figure 5. The extrapolated relationships of the maximum acceleration energy of muons depending on (a) the bubble's relativistic factor γ and (b) the relevant trapping energy threshold E_0 from the one-dimensional analytic model. The extrapolation of electrons (open circles) in the same parameters is also shown for comparison.

The E_0 and $E_{\rm acc}$ of muons at $t = 33$ ps are plotted in Figure 3(a). Clearly consistency and same trends exhibit as the expectation from the one-dimensional analytic model especially the sharp peaks of the lines denoting the trapping energy thresholds for different initial positions. The trapping energy thresholds are higher than the one-dimensional model estimations because the bubble structure distortion is not considered in the analytic model. Furthermore, in Figure 3(b), the energy spectra of both groups of muons are narrowed after the acceleration as expected.

4. Extrapolation of muon acceleration in laser wakefield

The good agreement of the one- and two-dimensional simulations gives us more confidence to extrapolate the estimation of muon acceleration. Obviously, to accelerate muons to higher energies, longer dephasing time is needed. Therefore the relativistic factor of the bubble γ would be the most important parameter in the extrapolation. The initial energy of muons E_0 is another important parameter for the finite muon energy from the 'Generator'. Considering the status of LWFA electrons up to now[15–20], we set the maximum $E_0 = 1.5$ GeV. With the one-dimensional analytic model, we estimate the extrapolated relationships of the maximum acceleration energies of muons $E_{\rm acc}$ depending on the bubble's relativistic factor $\gamma \in [10, 45]$ in Figure 5(a). For each setting of the bubble's relativistic factor γ, the relevant trapping energy threshold E_0 is different which is shown in Figure 5(b). We can see that giving the relativistic factor of the bubble $\gamma = 46$ and the initial energy $E_0 = 1.45$ GeV, the extrapolated maximum acceleration energy of muons could be up to 15.2 GeV. To obtain such high-energy muons, one needs to accelerate muons for 300 ps in the bubble's plasma channel (plasma density is $0.00045n_c$ and length 9 cm) which has been realized in the experiment[20]. To accelerate muons to more higher energy such as a Higgs

https://doi.org/10.1017/hpl.2018.65 Published online by Cambridge University Press

factory, a collision energy of around 125 GeV (muon energy 62.5 GeV) is needed which requires lower plasma density (plasma density is $0.00008n_c$ and length 46 cm) and higher relativistic factor ($\gamma \approx 110$) than the plasma channel in the literature. This kind of plasma channel has not been actualized but it might be realized in the future.

We have also shown the extrapolation of electron acceleration in the same parameters for comparison as the dashed line in Figure 5(a), in which we can find that the maximum acceleration of muons is larger than that of electrons by a factor of 2 to 3 for longer dephasing length. In fact, the dephasing length of trapped electrons reads[30]

$$L_{d-e} = \frac{v_e}{v_e - v_p} R \approx \frac{c}{c - v_p} R, \tag{3}$$

where v_e denotes the electron velocity, $R = \xi_R - \xi_L$ denotes the acceleration interval and v_p denotes the phase velocity of the bubble. Considering similar energy gain around GeV in the bubble, it is easily found that $v_e = c\sqrt{1 - \gamma^{-2}}$ is rapidly close to the speed of light c for electron energy larger than hundreds of MeV to GeV. However, for similar energy gain ΔE the relativistic factor $\gamma_\mu = \Delta E / m_\mu + 1$ of the muon is much smaller than that of electrons $\gamma_e = \Delta E / m_e + 1$ since the muon is more massive than the electron by 207 resulting $v_\mu < v_e \approx c$. Therefore, for the muon acceleration case the dephasing length reads

$$L_{d-\mu} = \frac{v_\mu}{v_\mu - v_p} R \approx \frac{c}{v_\mu - v_p} R, \tag{4}$$

where v_μ denotes the maximum velocity of muons. Therefore the dephasing length of muons is longer than that of electrons. Furthermore, the kinetic energy increase of charged particles in the rest frame of the bubble is $\bar{E}R$ which is same for electrons and muons. Here $\bar{E}$ is the average acceleration field in the bubble. However, the kinetic energy increase of charged particles in the lab frame is

$$\Delta E = \frac{\bar{E}R + v_p p'_x}{\sqrt{1 - \frac{v_p^2}{c^2}}} = \gamma \bar{E} R + \gamma v_p \sqrt{2 m_0 \bar{E} R}, \tag{5}$$

where $\gamma = (1 - v_p^2/c^2)^{1/2}$ is the relativistic factor of the bubble and $p'_x = \sqrt{2 m_0 \bar{E} R}$ is the momentum of the charged particle in the rest frame of the bubble. From Equation (5) we can find that the kinetic energy increase is strongly related to the invariant mass of the charged particle. Thus muons have higher energy gain compared to electrons on specific bubble setting.

5. Summary

Therefore, compared to electron or proton laser plasma accelerations, this all-optical muon acceleration scheme has particular characteristics. For the massive invariant mass, muons could be injected into the whole bubble acceleration region with a broader energy spread. Furthermore, higher energy gain compared to electrons could be achieved from the longer dephasing length. On the other hand, the light invariant mass decreases the trapping energy threshold which makes muons easier to catch up the bubble. Considering the crucial requirement of laser intensity for proton acceleration in the laser wakefield discussed in Ref. [31], muons (μ^+ and μ^-) are the feasible choice besides the electron and positron in LWFA mechanism based on the short pulse laser facilities now. Additionally, as an unstable particle, muon's lifetime 2.2 μs multiplied by the relativistic factor is long enough compared to the production and acceleration processes proposed in our scheme. Thus the decay losses could be neglected unlike traditional accelerator based muon production and acceleration processes. It is worth to mention that traditional accelerator muon sources are also suitable for the discussion here, but high time synchronization precision is needed.

In conclusion, we propose a new all-optical 'Generator and Booster' scheme to accelerate muons from the Bethe–Heitler dimuon production process by the laser wakefield to supply a prompt, compact, low cost and controllable muon source in the laser laboratories. To our knowledge, it is the first research on muon acceleration in the laser wakefield. By applying a one-dimensional analytic model, the muon trapping energy threshold depending on the phase space of the bubble region is discussed in detail. A two-dimensional PIC simulation is carried out to validate the acceleration picture. The forward and backward muons in the bubble region are simulated and well agreement with the one-dimensional estimation is presented. We also extrapolate the estimation to higher energy muon acceleration. It is shown that a maximum energy up to 15.2 GeV could be achieved with an initial energy $E_0 = 1.45$ GeV by accelerating muons for 300 ps with a bubble of relativistic factor $\gamma = 46$. This fact seems quite promising on existing short pulse laser facilities[32]. We expect such a new all-optical 'Generator and Booster' muon source to be realized in the near future.

Acknowledgements

The authors acknowledge Prof. H. B. Cai (IAPCM) for valuable discussions on this work. This work was supported by the Science Challenge Project (No. JCKY2016212A505) and the National Natural Science Foundation of China (No. 11805182).

References

1. C. Patrignani, K. Agashe, G. Aielli, C. Amsler, M. Antonelli, D. M. Asner, H. Baer, S. Banerjee, R. M. Barnett, T. Basaglia, C. W. Bauer, J. J. Beatty, V. I. Belousov, J. Beringer,

https://doi.org/10.1017/hpl.2018.65 Published online by Cambridge University Press

S. Bethke, H. Bichsel, O. Biebel, E. Blucher, G. Brooijmans, O. Buchmueller, V. Burkert, M. A. Bychkov, R. N. Cahn, M. Carena, A. Ceccucci, A. Cerri, D. Chakraborty, M.-C. Chen, R. S. Chivukula, K. Copic, G. Cowan, O. Dahl, G. D'Ambrosio, T. Damour, D. de Florian, A. de Gouvea, T. Degrand, P. de Jong, G. Dissertori, B. A. Dobrescu, M. Donofrio, M. Doser, M. Drees, H. K. Dreiner, D. A. Dwyer, P. Eerola, S. Eidelman, J. Ellis, J. Erler, V. V. Ezhela, W. Fetscher, B. D. Fields, B. Foster, A. Freitas, H. Gallagher, L. Garren, H.-J. Gerber, G. Gerbier, T. Gershon, T. Gherghetta, A. A. Godizov, M. Goodman, C. Grab, A. V. Gritsan, C. Grojean, D. E. Groom, M. Grunewald, A. Gurtu, T. Gutsche, H. E. Haber, K. Hagiwara, C. Hanhart, S. Hashimoto, Y. Hayato, K. G. Hayes, A. Hebecker, B. Heltsley, J. J. Hernández-Rey, K. Hikasa, J. Hisano, A. Höcker, J. Holder, A. Holtkamp, J. Huston, T. Hyodo, K. Irwin, J. D. Jackson, K. F. Johnson, M. Kado, M. Karliner, U. F. Katz, S. R. Klein, E. Klempt, R. V. Kowalewski, F. Krauss, M. Kreps, B. Krusche, Y. V. Kuyanov, Y. Kwon, O. Lahav, J. Laiho, P. Langacker, A. Liddle, Z. Ligeti, C.-J. Lin, C. Lippmann, T. M. Liss, L. Littenberg, K. S. Lugovsky, S. B. Lugovsky, A. Lusiani, Y. Makida, F. Maltoni, T. Mannel, A. V. Manohar, W. J. Marciano, A. D. Martin, A. Masoni, J. Matthews, U.-G. Meiner, D. Milstead, R. E. Mitchell, P. Molaro, K. Monig, F. Moortgat, M. J. Mortonson, H. Murayama, K. Nakamura, M. Narain, P. Nason, S. Navas, M. Neubert, P. Nevski, Y. Nir, K. A. Olive, S. Pagan Griso, J. Parsons, J. A. Peacock, M. Pennington, S. T. Petcov, V. A. Petrov, A. Piepke, A. Pomarol, A. Quadt, S. Raby, J. Rademacker, G. Raffelt, B. N. Ratcliff, P. Richardson, A. Ringwald, S. Roesler, S. Rolli, A. Romaniouk, L. J. Rosenberg, J. L. Rosner, G. Rybka, R. A. Ryutin, C. T. Sachrajda, Y. Sakai, G. P. Salam, S. Sarkar, F. Sauli, O. Schneider, K. Scholberg, A. J. Schwartz, D. Scott, V. Sharma, S. R. Sharpe, T. Shutt, M. Silari, T. Sjostrand, P. Skands, T. Skwarnicki, J. G. Smith, G. F. Smoot, S. Spanier, H. Spieler, C. Spiering, A. Stahl, S. L. Stone, Y. Sumino, T. Sumiyoshi, M. J. Syphers, F. Takahashi, M. Tanabashi, K. Terashi, J. Terning, R. S. Thorne, L. Tiator, M. Titov, N. P. Tkachenko, N. A. Tornqvist, D. Tovey, G. Valencia, R. Van de Water, N. Varelas, G. Venanzoni, M. G. Vincter, P. Vogel, A. Vogt, S. P. Wakely, W. Walkowiak, C. W. Walter, D. Wands, D. R. Ward, M. O. Wascko, G. Weiglein, D. H. Weinberg, E. J. Weinberg, M. White, L. R. Wiencke, S. Willocq, C. G. Wohl, L. Wolfenstein, J. Womersley, C. L. Woody, R. L. Workman, W.-M. Yao, G. P. Zeller, O. V. Zenin, R.-Y. Zhu, F. Zimmermann, and P. A. Zyla, Chin. Phys. C **40**, 100001 (2016).
2. F. J. M. Farley and Y. K. Semertzidis, Prog. Part. Nucl. Phys. **52**, 1 (2004).
3. R. B. Palmer, Rev. Acc. Sci. Tech. **7**, 137 (2014).
4. P. Ackerbauer, J. Werner, W. H. Breunlich, M. Cargnelli, S. Fussy, M. Jeitler, P. Kammel, J. Marton, A. Scrinzi, J. Zmeskal, J. Bistirlich, K. M. Crowe, J. Kurck, C. Petitjean, R. H. Sherman, H. Bossy, H. Daniel, F. J. Hartmann, W. Neumann, G. Schmidt, and M. P. Faifman, Nucl. Phys. A **652**, 311 (1999).
5. S. J. Blundell, Contemp. Phys. **40**, 175 (1999).
6. K. N. Borozdin, G. E. Hogan, C. Morris, W. C. Priedhorsky, A. Saunders, L. J. Schultz, and M. E. Teasdale, Nature **422**, 277 (2003).
7. K. Nagamine, *Introductory Muon Science* (Cambridge University Press, 2003).
8. A. Carne, S. F. J. Cox, G. H. Eaton, and C. A. Scott, Hyperfine Interact. **65**, 1175 (1990).
9. Y. Miyake, K. Nishiyama, N. Kawamura, P. Strasser, S. Makimura, A. Koda, K. Shimonura, H. Fujimori, K. Nakahara, R. Kadono, M. Kato, S. Takeshita, W. Higemoto, K. Ishida, T. Matsuzaki, Y. Matsuda, and K. Nagamine, Nucl. Instrum. Methods A **600**, 22 (2009).
10. A. Rafeal, B. X. Donath, D. Herlach, D. Maden, I. D. Reid, D. Renker, G. Solt, and U. Zimmermann, Hyperfine Interact. **87**, 1105 (1994).
11. G. M. Marshall, Z. Phys. C **56**, s226 (1992).
12. E. Esarey, C. B. Schroeder, and W. P. Leemans, Rev. Mod. Phys. **81**, 1229 (2009).
13. W. Lu, C. Huang, M. Zhou, W. B. Mori, and T. Katsouleas, Phys. Rev. Lett. **96**, 165002 (2006).
14. A. I. Titov, B. Kampfer, and H. Takabe, Phys. Rev. Spec. Top. Accel. Beams **12**, 111301 (2009).
15. W. P. Leemans, B. Nagler, A. J. Gonsalves, C. Toth, K. Nakamura, C. G. R. Geddes, E. Esarey, C. B. Schroeder, and S. M. Hooker, Nat. Phys. **2**, 696 (2006).
16. N. Hafz, T. Jeong, I. Chol, S. Lee, K. Pae, V. Kulagin, T. Yu, K. Hong, T. Hosokai, J. R. Cary, D. Ko, and J. Lee, Nat. Photonics **2**, 571 (2008).
17. C. E. Clayton, J. E. Ralph, F. Albert, R. A. Fonseca, S. H. Glenzer, C. Joshi, W. Lu, K. A. Marsh, S. F. Martins, W. B. Mori, A. Pak, F. S. Tsung, B. B. Pollock, J. S. Ross, L. O. Silva, and D. H. Froula, Phys. Rev. Lett. **105**, 105003 (2010).
18. H. T. Kim, K. H. Pae, H. J. Cha, I. J. Kim, T. J. Yu, J. H. Sung, S. K. Lee, T. M. Jeong, and J. Lee, Phys. Rev. Lett. **111**, 165002 (2013).
19. X. M. Wang, R. Zgadzaj, N. Fazel, Z. Li, S. A. Yi, X. Zhang, W. Henderson, Y. Y. Chang, R. Korzekwa, H. E. Tsai, C. H. Pai, H. Quevedo, G. Dyer, E. Gaul, M. Martinez, A. C. Bernstein, T. Borger, M. Spinks, M. Donovan, V. Khudik, G. Shvets, T. Ditmire, and M. C. Downer, Nat. Commun. **4**, 1988 (2013).
20. W. P. Leemans, A. J. Gonsalves, H. S. Mao, K. Nakamura, C. Benedetti, C. B. Schroeder, C. Toth, J. Daniels, D. E. Mittelberger, S. S. Bulanov, J. L. Vay, C. G. R. Geddes, and E. Esarey, Phys. Rev. Lett. **113**, 245002 (2014).
21. F. Zhang, B. Y. Li, L. Q. Shan, B. Zhang, W. Hong, and Y. Q. Gu, High Power Laser Sci. Eng. **5**, e16 (2017).
22. S. R. Klein, R. Mikkelsen, and J. K. B. Tjus, Astrophys. J. **779**, 106 (2013).
23. F. Peano, J. Vieira, R. Mulas, G. Coppa, R. Bingham, and L. O. Silva, Plasma Phys. Control. Fusion **51**, 024006 (2009).
24. S. Steinke, J. van Tilborg, C. Benedetti, C. G. R. Geddes, C. B. Schroeder, J. Daniels, K. K. Swanson, A. J. Gonsalves, K. Nakamura, N. H. Matlis, B. H. Shaw, E. Esarey, and P. Leemans, Nature **530**, 190 (2016).
25. S. A. Kahn, S. Korenev, M. Bishai, M. Diwan, J. C. Gallardo, A. Hershcovitch, and B. M. Johnson, in *11th European Particle Accelerator Conference (EPAC 08)* (2008), paper MOPP073.
26. J. Teng, Y. Q. Gu, J. Chen, B. Zhu, T. K. Zhang, F. Tan, W. Hong, B. H. Zhang, and X. Q. Wang, Nucl. Instrum. Methods Phys. Res. A **826**, 15 (2016).
27. W. Leemans and E. Esarey, Phys. Today **62**, 44 (2009).
28. W. Song, R. H. Hu, Y. R. Shou, Z. Gong, J. Q. Yu, C. Lin, W. J. Ma, Y. Y. Zhao, H. Y. Lu, and X. Q. Yan, Chin. Phys. Lett. **34**, 085201 (2017).
29. J. B. Rosenzweig, A. M. Cook, A. Scott, M. C. Tompson, and R. B. Yoder, Phys. Rev. Lett. **95**, 195002 (2005).
30. W. Lu, M. Tzoufras, C. Joshi, F. S. Tsung, W. B. Mori, J. Vieira, R. A. Fonseca, and L. O. Silva, Phys. Rev. Spec. Accel. Beams **10**, 061301 (2007).
31. B. Shen, Y. Li, M. Y. Yu, and J. Cary, Phys. Rev. E **76**, 055402(R) (2007).
32. C. Danson, D. Hillier, N. Hopps, and D. Neely, High Power Laser Sci. Eng. **3**, e3 (2015).

https://doi.org/10.1017/hpl.2018.65 Published online by Cambridge University Press